Compressed Sensing Reconstruction for Magnetic Resonance Parameter Mapping

Mariya Doneva,[1]* Peter Börnert,[2] Holger Eggers,[2] Christian Stehning,[2] Julien Sénégas,[2] and Alfred Mertins[1]

Compressed sensing (CS) holds considerable promise to accelerate the data acquisition in magnetic resonance imaging by exploiting signal sparsity. Prior knowledge about the signal can be exploited in some applications to choose an appropriate sparsifying transform. This work presents a CS reconstruction for magnetic resonance (MR) parameter mapping, which applies an overcomplete dictionary, learned from the data model to sparsify the signal. The approach is presented and evaluated in simulations and in in vivo T_1 and T_2 mapping experiments in the brain. Accurate T_1 and T_2 maps are obtained from highly reduced data. This model-based reconstruction could also be applied to other MR parameter mapping applications like diffusion and perfusion imaging. Magn Reson Med 64:1114–1120, 2010. © 2010 Wiley-Liss, Inc.

Key words: MRI; image reconstruction; compressed sensing; T_1 mapping; T_2 mapping

Different tissues in the human body can be distinguished in magnetic resonance imaging (MRI) by their intrinsic magnetic resonance (MR) parameters, such as proton density, longitudinal (T_1) and transversal (T_2) relaxation times (1). Direct quantification of the local MR parameters is of interest in a wide range of clinical applications including oncology and neurology (2,3), because it often provides more accurate and reproducible diagnostic information.

A major concern in MR parameter mapping is the often long scan time. This has led to an estimation of T_1 and T_2 relaxation times from three or even only two data points, which entails poor accuracy and does not give any indication of multicompartmental signal behavior. Higher numbers of measurements are necessary to cover a large dynamic range of tissue parameters relevant in clinical applications (4) and also to improve the accuracy of the fit and SNR. Multiexponential fits can be applied to decrease partial volume effects and to characterize multicompartmental relaxation curves (5). Several works consider measurements of T_2 distributions in tissue acquiring several thousand echoes (6,7).

This article presents a technique for reducing the acquisition time in multipoint MR parameter mapping experiments, which is inspired by the theory of compressed sensing (CS) (8,9). The framework of CS is a promising concept for exploiting signal sparsity to accelerate the data acquisition. The underlying sparsifying transforms are often chosen with very few assumptions about the MR signal. Finite differences and wavelet transforms assume, for instance, that most medical images are piecewise smooth or have sparse wavelet representations. The reconstruction could be better tailored to the specific problem if data-specific transforms were used. For example, in dynamic imaging, sparsity along the temporal dimension is promoted by subtracting a composite image or applying a Fourier transform in case of periodic motion (10,11).

In this work, the prior knowledge of the data model in MR parameter mapping is used to design an overcomplete dictionary, which is applied to sparsify the data in CS image reconstruction. The method is demonstrated in simulations and in in vivo T_1 and T_2 mapping applications.

METHODS

In the following, we will consider the framework of a generalized MR parameter mapping problem. Given an underlying model $f(p;\boldsymbol{\theta})$, a spatially resolved estimation of the parameters of interest $\boldsymbol{\theta}$ requires the acquisition of several images at different values of the encoding parameter p. A typical data acquisition scheme with Cartesian sampling is shown in Fig. 1. We will refer to this measurement space as k–p space. Scan time reduction can be achieved by undersampling in the phase-encoding (k_y) and parameter-encoding (p) dimensions.

Compressed Sensing

CS (8,9) allows for accurate signal reconstruction from a small number of linear measurements by exploiting signal sparsity. Finding the optimal solution for the signal $\mathbf{x}$ involves solving the ℓ_0 minimization problem

$$\text{minimize } \|\boldsymbol{\Psi}\mathbf{x}\|_0, \text{ subject to } \|\mathbf{y}-\boldsymbol{\Phi}\mathbf{x}\|_2 \leq \epsilon, \qquad [1]$$

where $\boldsymbol{\Psi}$ is the sparsifying transform, $\mathbf{y}$ is the measurement vector, $\boldsymbol{\Phi}$ is the measurement matrix, and ϵ is related to the signal noise level. Although this problem is computationally intractable, different techniques have been developed that give a very accurate and sometimes even exact solution of Eq. [1] (12–14).

Sparsity: Model-Based Transform

Most commonly, orthonormal bases are applied as sparsifying transforms for CS. However, representing a signal with respect to an overcomplete dictionary adds more flexibility in the signal representation and could significantly

[1]Institute for Signal Processing, University of Luebeck, Luebeck, Germany
[2]Philips Research Europe - Hamburg Tomographic Imaging Department, Hamburg, Germany
*Correspondence to: Mariya Doneva, University of Luebeck, Ratzeburger Allee 160, 23538 Luebeck, Germany. E-mail: mariya.doneva@isip.uni-luebeck.de
Received 28 August 2009; revised 8 February 2010; accepted 17 March 2010.
DOI 10.1002/mrm.22483
Published online 17 June 2010 in Wiley Online Library (wileyonlinelibrary.com).

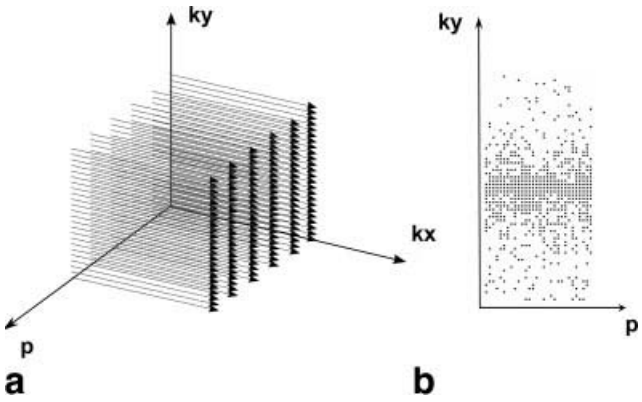

FIG. 1. Data acquisition in Cartesian k–p space. (**a**) Conventional sampling where a full Cartesian dataset is acquired for each parameter-encoding value p with arrows indicating the readout dimension. (**b**) Incoherent sampling for compressed sensing, achieved by variable density random undersampling in k–p space [on the Cartesian grid given in (**a**)]. Acquired data points in the k_y–p plane are shown in black (with readout orthogonal to the drawing plane).

improve sparsity. A dictionary is a collection of discrete-time signal prototypes (atoms) and is overcomplete if the number of atoms is greater than the signal dimensionality. Large data-adapted dictionaries allow for accurate data description with just a few atoms and in this way achieve much sparser representations compared with orthonormal bases. Knowledge of the data model allows us to generate a set of signal prototypes by evaluating the model for a discrete set of parameters. This set of prototype signals characterizes the data dependencies within the model and could be used as a training set to design a model-based dictionary. Generating the training set requires only knowledge of the model and the expected range of the parameters, but no previously measured data are necessary.

An overcomplete dictionary that sparsely represents the training data can be designed by the K-SVD method proposed by Aharon et al. (15). The K-SVD algorithm works iteratively, applying two steps in each iteration: (1) in the sparse coding step, the dictionary $\mathbf{D}$ is fixed, and a sparse representation with respect to that dictionary is obtained; (2) in the dictionary update step, the dictionary columns are updated, one column at a time to minimize the approximation error of the training data. The learned dictionary is optimized for a signal approximation with at most K atoms. The value of K is chosen as small as possible, such that the approximation error in the learned dictionary is below a given threshold, e.g., 10^{-5}.

The K-term representation of a signal $\mathbf{x}$ with respect to a dictionary $\mathbf{D}$ requires solving the problem:

$$\text{minimize } \|\mathbf{x} - \mathbf{D}\mathbf{s}\|_2, \text{ subject to } \|\mathbf{s}\|_0 \leq K. \qquad [2]$$

This problem can be efficiently solved using orthogonal matching pursuit (OMP) (16). The model-based dictionary is applied in the parameter-encoding dimension p. However, each one-dimensional signal in the parameter dimension is related to the complete k–p dataset, requiring joint estimation of the complete dataset. Further sparsity in the image domain can be imposed by applying wavelets or finite differences.

Sampling and Incoherence

The sampling pattern considered in this article is illustrated in Fig. 1b. Random undersampling in k_y–p (on a Cartesian grid) is performed with variable sampling density in k_y, accounting that most energy of MR images is concentrated in the low frequencies, and with uniform density in p. This choice is mainly motivated by its compatibility with multiecho acquisition sequences. Alternatively, the sampling density in p can be adapted to the signal distribution. Incoherence plays an important role in CS and sparse signal approximation. Low-coherence guarantees that sparse recovery algorithms can exactly recover any sufficiently sparse signal and that this solution is unique. In CS, incoherence of the measurement matrix (related to the sampling in k–p space) is desired. The proposed sampling pattern in k–p space results in noise-like artifacts in both the image and the parameter dimensions, which can be removed in the reconstruction. Incoherence is also desired for the dictionary $\mathbf{D}$ in the sparse approximation problem in Eq. [2]. The model-based dictionary may have high coherence, caused by the correlations between signals with different parameters values, so it is not generally optimal. However, empirical results show that very accurate sparse signal approximation can be obtained for signals drawn from the data model, therefore enabling accurate reconstruction.

Reconstruction

Given a measurement vector $\mathbf{y}$ in k–p space, the goal is to reconstruct the image series $\mathbf{x}$, consisting of L images $\mathbf{x}_l$ at parameter-encoding values p_l, $l = 1, \ldots, L$. The signal in the parameter dimension at voxel n is denoted with $\mathbf{x}_n$, where $n = 1, \ldots, N$, and N is the number of voxels. The sparsity parameter K in the dictionary representation is estimated during the dictionary training phase and is fixed. The K-term estimate is obtained using OMP. The complete data $\mathbf{x}$ are jointly reconstructed, applying the following iterative procedure:

Set $\mathbf{y}^{(0)} = \mathbf{y}$, $\mathbf{x}^{(0)} = \mathbf{0}$. For iteration i:

1. Apply $\mathbf{x}_l^{(i)} = \mathcal{F}_u^H \mathbf{y}_l^{(i-1)}$ for $l = 1, \ldots, L$
2. Compute the K-term estimate $\mathbf{x}_n^{(i)} = \mathbf{D}\mathbf{s}_n^{(i)}$, $\|\mathbf{s}_n^{(i)}\|_0 = K$, $n = 1, \ldots, N$
3. Compute $\mathbf{y}_l^{(i)} = \mathcal{F}_u \mathbf{x}_l^{(i)}$ for $l = 1, \ldots, L$ and insert the measured data at the sampling locations $\mathbf{y}^{(i)} = \mathbf{y}|_{\text{acq}}$
4. Repeat Steps 1–3 until the change of energy in $\mathbf{x}$ gets smaller than a given threshold $\frac{\|\mathbf{x}^{(i)} - \mathbf{x}^{(i-1)}\|}{\|\mathbf{x}^{(i)}\|} < \epsilon$

Here $\mathcal{F}_u$ is the undersampled Fourier operator and H denotes the Hermitian conjugate.

Additional sparsity in the images can be exploited, for instance, by including the following step, denoted as 2′. Compute $\mathbf{x}_l^{(i)} = \mathbf{\Psi}^{-1}\mathcal{T}(\mathbf{\Psi}\mathbf{x}_l^{(i)}, t_l)$, $l = 1, \ldots, L$, where $\mathcal{T}$ is the soft thresholding operation and $\mathbf{\Psi}$ is a wavelet transform.

The extended algorithm applies Steps 2 and 2′ alternately during the iterations. The threshold t is determined according to estimation of the signal sparsity. Three variants

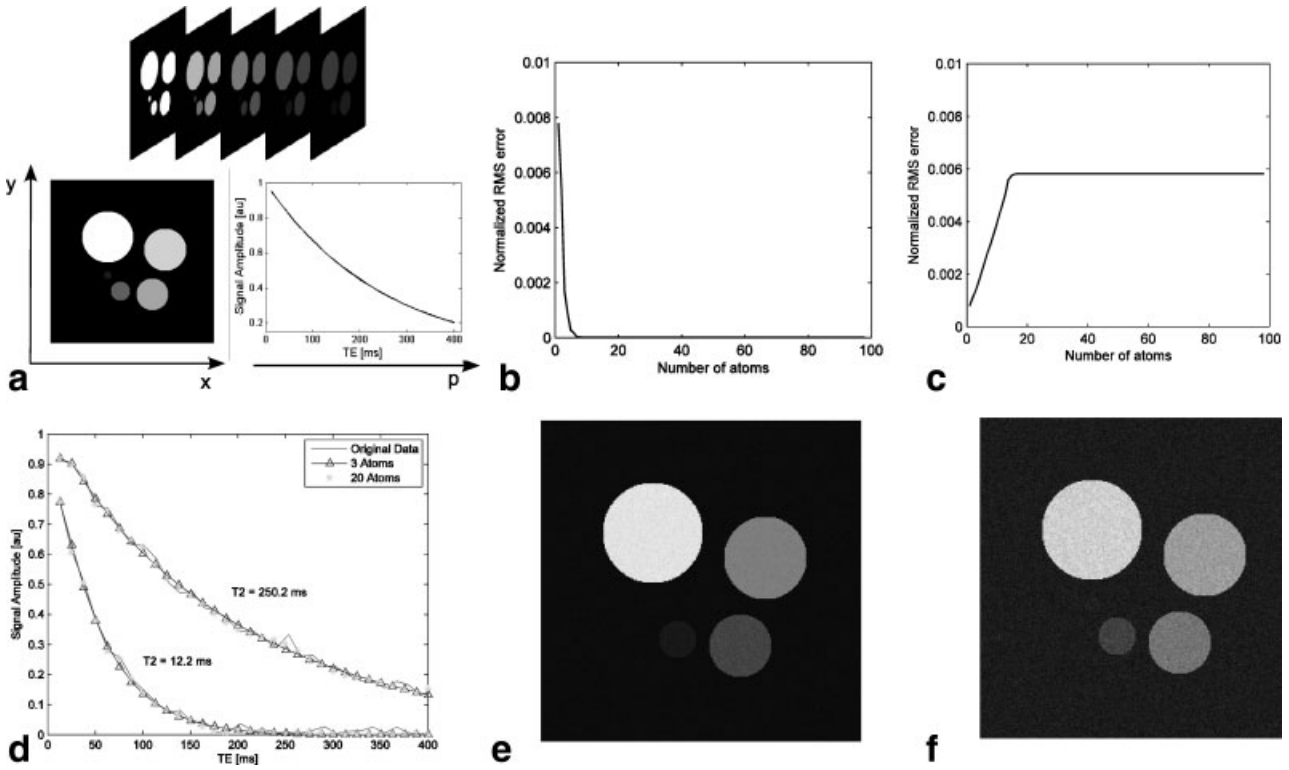

FIG. 2. Signal approximation with the model-based dictionary. The phantom used in simulations to test the ability of the dictionary to approximate data is shown in (**a**). The NRMSE as a function of the number of dictionary atoms used in the approximation is shown for (**b**) noiseless and (**c**) noisy data. The transform achieves a very good signal approximation of noiseless data with few atoms. Applied to noisy data, most of the signal is contained in the first few atoms, and the noise is partly approximated by adding further atoms. The signal in the temporal dimension and its approximation with 3 and 20 atoms for low and high T_2 values is shown in (**d**). The corresponding images for TE = 250 msec are shown in (**e**) and (**f**) for an approximation with 3 and 20 atoms, respectively.

were studied: **A:** Apply the model-based dictionary in the parameter-encoding dimension and wavelets (Daubechies 4) on the images. **B:** Apply only the dictionary in the parameter-encoding dimension. **C:** Apply wavelets on the images and in the parameter-encoding dimension. **A** is the recommended approach, **B** shows the performance of the model-based dictionary alone, and **C** is the classical approach, using a general transform instead of the dictionary.

Data Model

In this work, model-based CS reconstruction is applied to accelerate T_1 and T_2 measurements. The detectable MR signal M in these and some other measurements (e.g., diffusion) can be described by the exponential model

$$M(p) = \alpha + \beta \exp(-p/\tau), \quad [3]$$

where τ denotes the tissue parameter in question and α and β are complex parameters, which are also estimated in the fit. The sampling locations of p are determined by the expected range of the relaxation parameters. Uniform sampling with $p_{\max}$ equal to two times the target value of τ is a common choice.

Simulations

To demonstrate the ability of the overcomplete dictionary to sparsely represent data and account for the effects of noise, a computer model was implemented mimicking a T_2 mapping experiment. The simulated phantom (Fig. 2a) consisted of 32 images with echo time (TE) spacing of 12.5 msec and matrix size of 256×256 and contained five compartments, with different T_2 values (12–250 msec). Gaussian noise with $\sigma = 0.02$ [signal-to-noise ratio (SNR) = 50] was added to simulate noisy data. A training set of 1,000 exponentials was generated with decay coefficients uniformly distributed between 1 and 300 msec. A dictionary with 100 atoms was learned using K-SVD, optimized for sparsity $K = 3$. The T_2 values of the phantom data were not contained in the training set. A signal approximation with respect to the dictionary was obtained with increasing number of atoms using OMP. The normalized root mean square error (NRMSE) was used as a quality measure of the approximation. The simulation data were undersampled with various reduction factors (2–8) and reconstructed with each of the reconstruction variants, described above. Parameter maps were obtained from the set of images on a voxel-by-voxel basis using the Levenberg–Marquardt algorithm.

Measurements

T_1 and T_2 data in the brain were acquired in healthy volunteers with informed consent obtained. Measurements were performed on a 1.5 T clinical scanner (Achieva, Philips Healthcare).

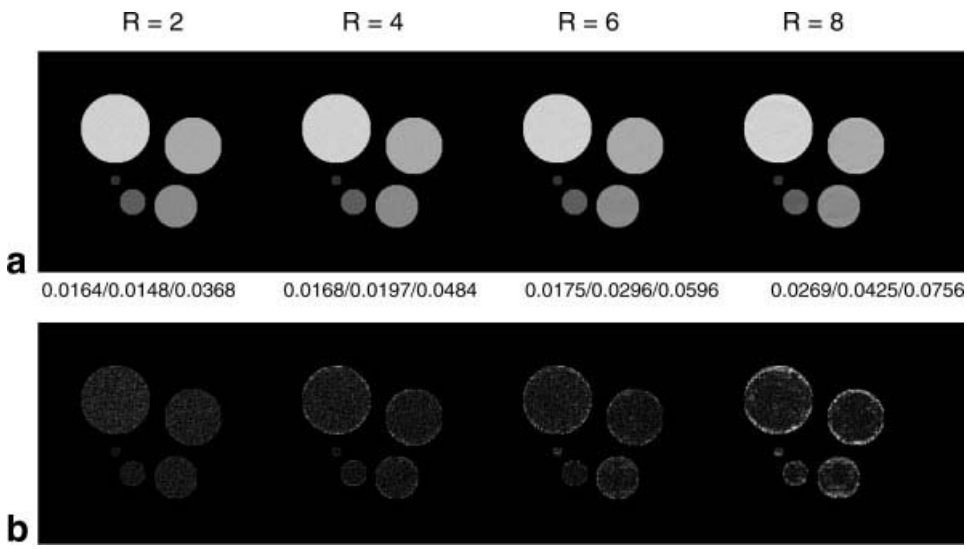

FIG. 3. CS reconstruction of simulated data in the presence of noise. Parameter maps obtained from image series reconstructed with the proposed model-based reconstruction (reconstuction variant **A**) are shown for different undersampling factors in (**a**). The NRMSE for the three reconstruction variants is given in the following order: dictionary and wavelets/dictionary only/wavelets in the image and the parameter dimensions (reconstruction variants **A**/**B**/**C**). Note that a conventional parameter mapping reconstruction using fully sampled data results in a NRMSE of 0.0179 because of the finite SNR in the data. The corresponding error maps are shown in (**b**).

For T_1 mapping, inversion recovery data were acquired with a Look-Locker sequence including a correction for apparent T_1 values (17). The following parameters were used for the measurement: 40 inversion time increments, ΔT_i = 72 msec, inversion repetition time (TR) 3 sec, FOV 250×250 mm, 7-mm slice thickness, 224×224 matrix. The data at each inversion time were acquired with a segmented gradient echo sequence (TE = 1.9 msec, TR = 3.8 msec, flip angle 10°). For T_2 mapping, multi-spin-echo measurements were performed with the following parameters: 32 echoes, 5 msec echo spacing, FOV 250 × 250 mm, 6-mm slice thickness, 256 × 256 matrix, TR = 1 sec.

The datasets were undersampled retrospectively with reduction factors of 2, 4, 6, and 8 for the T_1 and 2, 3, 4, and 5 for the T_2 dataset. The undersampled data were reconstructed with each of the three variants described above. A dictionary consisting of 100 atoms was trained for each model. The training dataset for the T_1 model consisted of 2,500 exponentials corresponding to apparent T_1 values between 0.2 and 500 msec. The dataset for the T_2 model consisted of 1,000 exponentials with decay constants between 1 and 300 msec.

The reconstructed image series and the resulting maps were compared with results obtained with full sampling. To assess the reconstruction quality, the NRMSE was calculated for the reconstructed image series and the corresponding parameter maps for each reconstruction case.

RESULTS

Simulations

The approximation error as a function of the number of dictionary atoms is shown in Fig. 2. In the noiseless case, very accurate signal approximation is achieved with two or three atoms (Fig. 2b). Approximation of noisy data shows that the dictionary is very discriminative to noise. With increasing number of atoms some of the noise is approximated, however, a large portion is discarded (Fig. 2c). This denoising effect can be seen in the parameter dimension (Fig. 2d) and in the images for approximation with 3 (Fig. 2e) and 20 (Fig. 2f) atoms.

Figures 3–5 show the images from the undersampling experiments for the best reconstruction variant (**A**, applying both the model-based dictionary and wavelets). The NRMSE for all three reconstruction variants is indicated in the figures.

Figure 3 shows the maps obtained from the CS reconstructed image series of the simulation dataset. Accurate parameter maps were obtained for all reduction factors. The error for reduction factor of 6 is about the same as for the map obtained from 32 fully sampled echoes (0.0179), as a consequence of the finite SNR. The denoising effect of the reconstruction results in decreased errors for lower reduction factors. With increasing reduction factor, the error in the maps changes from noise-like to localized (artifacts).

Measurements

Figure 4 shows selected results from the in vivo T_1 mapping experiments. A single image picked from the acquired image series is shown for full Nyquist sampling and for CS reconstruction with reduction factors of 2–8. As expected, a slight denoising is observed in the CS reconstructed images. All visible artifacts in the images, resulting from the undersampling, could be removed for a reduction factor up to 6. For higher reduction factors, some residual aliasing and blurring are observed in the reconstructed images (Fig. 4, $R = 8$). The resulting T_1 maps are shown in Fig. 4b. The quality of the maps corresponds well to the quality of the image series.

Results from the T_2 mapping experiments are shown in Fig. 5. Accurate reconstruction was achieved for data reduction factors up to 4. For higher reduction factors, the image quality is visibly decreased. Images for all three reconstruction cases are shown in Fig. 5 for the example of $R = 3$. The images, reconstructed with the dictionary only (Fig. 5c) appear "more grainy," compared with the case when wavelets in the image domain are applied additionally. The reconstruction using wavelets only (Fig. 5d) shows significant artifacts already at $R = 3$.

The reconstruction case **A** shows the smallest NRMSE in all experiments. Applying the dictionary alone results in

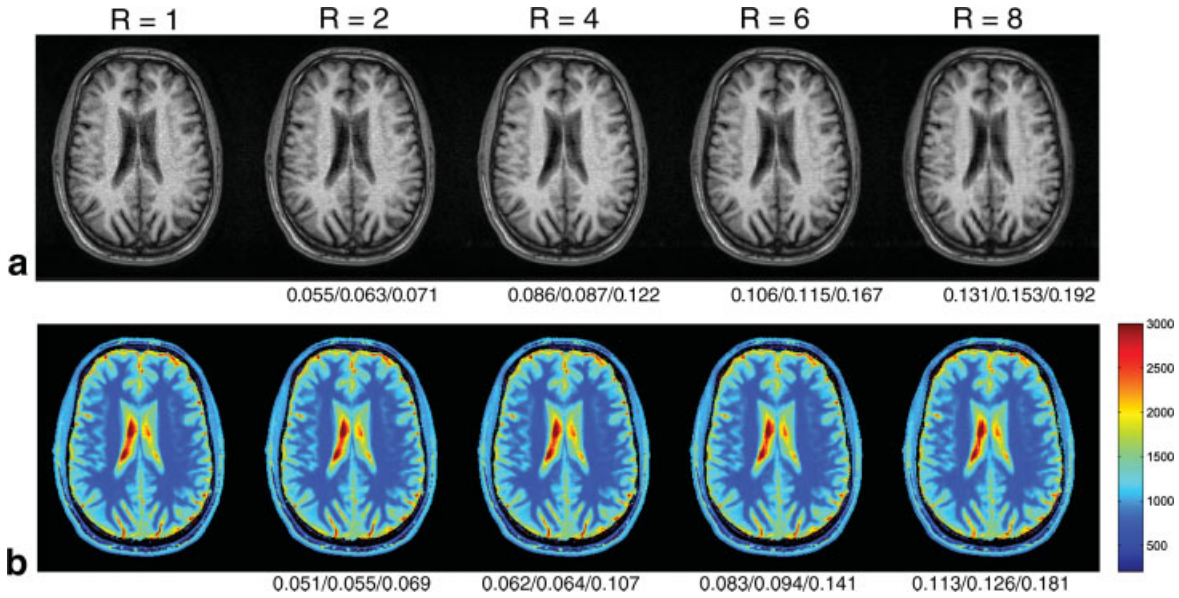

FIG. 4. CS reconstruction of T_1 mapping data applying a model-based dictionary. (**a**) Images for TI = 1.65 sec and full sampling ($R = 1$) and CS reconstruction with various reduction factors ($R = 2, \ldots, 8$). Slight denoising is observed in the CS-reconstructed images. (**b**) The resulting T_1 maps do not show any visible differences compared with the reference map up to a reduction factor of 6. The NRMSE with respect to the fully sampled image/map is given below each image/map for all reconstruction variants **A**/**B**/**C**. The color-coding bar indicates the T_1 times in msec.

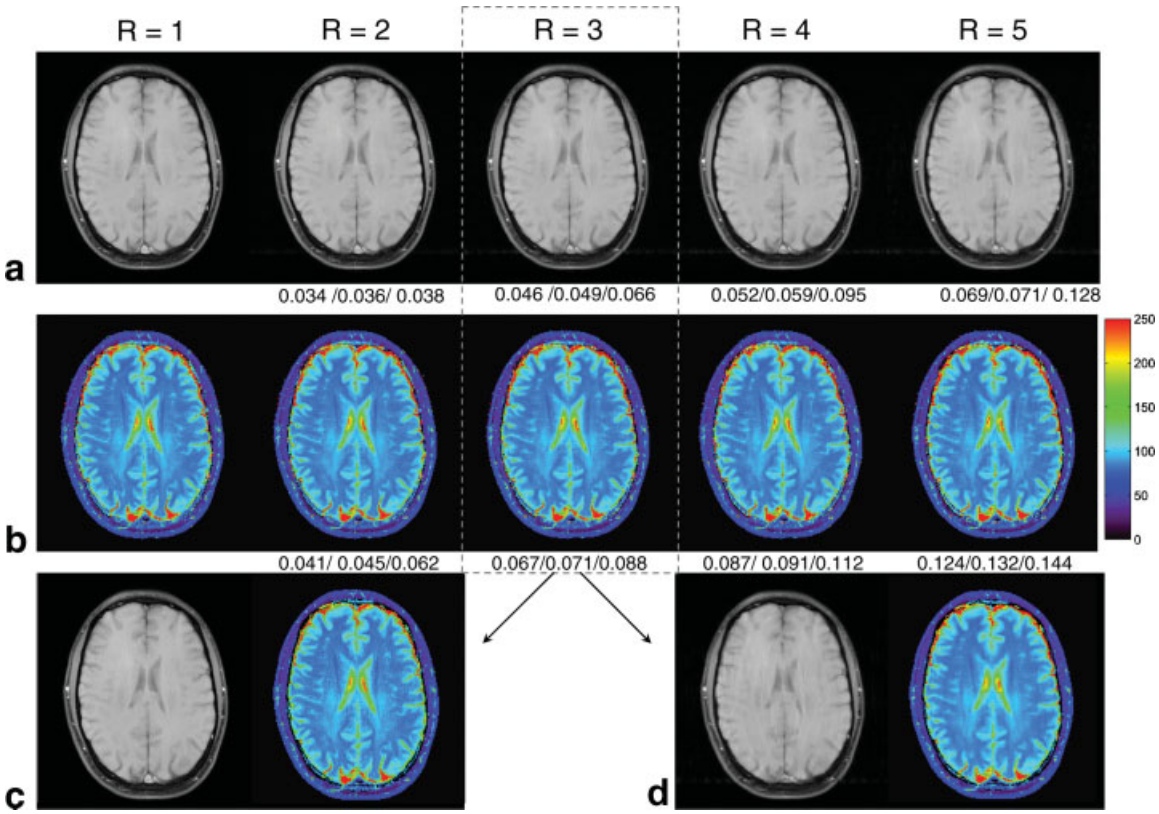

FIG. 5. CS reconstruction of T_2 mapping data with model-based dictionary. (**a**) Image for TE = 20 msec full sampling ($R = 1$) and CS reconstruction with reduction factors 2–5. (**b**) The corresponding T_2 maps. The color-coding bar indicates the T_2 times in milliseconds. The NRMSE with respect to the fully sampled data is given below each image for all reconstruction variants (**A**/**B**/**C**). (**c**, **d**) The images for $R = 3$ using the dictionary only and wavelets only are shown respectively.

similar reconstruction quality for most of the cases. Significant improvement of using both transforms together has only been achieved in the phantom experiments. In all experiments, the standard reconstruction (**C**) shows artifacts for a reduction factors above 2.

The number of required iterations was between 6 and 35 depending on the reduction factor. The computation time for one iteration was about 29 sec for a $256 \times 256 \times 32$ matrix (Matlab, 2.2 GHz CPU).

DISCUSSION

We have presented a CS reconstruction method that attains an accurate reconstruction from highly undersampled data in MR parameter mapping. Prior knowledge of the signal model was incorporated in the reconstruction by applying an overcomplete dictionary, learned from the data model as a sparsity transform. The method was applied in T_1- and T_2-mapping experiments, achieving acceleration factors of about 4–6, which is a great improvement over general transforms such as wavelets. Applying an additional sparsity constraint in the wavelet domain can further improve the reconstruction, mostly for images with very sparse wavelet representation. The achievable reduction factors may vary for different datasets depending on data compressibility, data size, sampling pattern, SNR, or potential deviations from the model.

The sparsity of the signal representation with respect to an overcomplete dictionary depends on the training data and on the dictionary size. Generally, the sparsity can be improved by increasing the dictionary size but this also increases the computational burden and the dictionary coherence. Although the model-based dictionary may have high coherence, we have obtained surprisingly good sparse signal approximation with OMP, and, as a consequence, a good CS reconstruction. Because of the high redundancy, also signals with parameter values not included in the training set are described very sparsely. Furthermore, the dictionary is very discriminative and gives a very poor representation of signals unrelated to the model and noise. This allows efficient reduction of the incoherent artifacts and improved reconstruction. Similar observations have been reported in (18), showing clear advantage of coherent dictionaries in the signal recovery from randomly corrupted images. An incoherent dictionary (orthogonal basis) can be learned from the model using principal component analysis (PCA) (19), however the sparsity in such dictionary is worse.

In a dictionary with infinitely many atoms, the signal can be ultimately represented by a single atom. This is equivalent to fitting the signal to the model. Thus, another possible reconstruction approach would be to fit the undersampled data to the model at each iteration and subtract the artifacts from the resulting signal approximation. Another related approach would be to combine the CS reconstruction with a nonlinear inversion approach (20), jointly estimating the images and the parameter map. These two approaches could be an interesting alternative to the one proposed here; however, they involve a nonlinear sparsifying transform or nonlinear measurements, which are not considered in the existing CS theory. Furthermore, there might be difficulties regarding numerical stability due to the nonlinearity and multiple local minima as well as increased computational complexity.

The presented model-based transform does not restrict the signal to a single exponential. In fact, the reconstructed signal is a linear combination of multiple exponentials, so the reconstruction is also compatible with a multiexponential fit. Therefore, multiple relaxation components in a heterogeneous voxel can be assessed. The model-based reconstruction method was demonstrated for the applications of accelerated T_1 and T_2 mapping in the brain. Further applications include diffusion imaging and potentially more complex MR tissue signal models, as for instance contrast agent uptake and perfusion.

Several other methods exist to speed up sampling in MRI. Such methods, for instance, are partial *k*-space sampling, exploiting the conjugate symmetry of the Fourier transform of real images, and parallel imaging. A combination with these methods could potentially allow even higher data reduction and thus higher acceleration factors.

CONCLUSIONS

In this article, we introduced a model-based reconstruction that applies a learned overcomplete dictionary to sparsify the data and applied it to MR relaxation parameter mapping. It proved superior to a reconstruction with general transforms, such as wavelets, and produced accurate results at higher reduction factors. This advantage may be exploited to accelerate MR parameter mapping, or to increase the spatial or temporal resolution, given a constant scan time. Further studies are needed to expand the scope of possible MR parameters that can be addressed with this approach.

REFERENCES

1. Bottomley P, Hardy C, Argersinger R, Allen-Moore G. A review of 1H NMR relaxation in pathology: Are T1 and T2 diagnostic? Med Phys 1987;14:1–37.
2. Warntjes JBM, Dahlqvist Leinhard O, West J, Lundberg P. Rapid magnetic resonance quantification on the brain: Optimization for clinical usage. Magn Reson Med 2008;60:320–329.
3. Tofts P. Quantitative MRI of the brain: measuring change caused by disease. Chichester, UK: John Wiley & Sons; 2003.
4. Crawley A, Henkelman R. A comparison of one-shot and recovery methods in T1 imaging. Magn Reson Med 1988;7:23–34.
5. Kroeker R, Henkelman R. Analysis of biological NMR relaxation data with continuous distributions of relaxation times. J Magn Reson 1986;69:218–235.
6. Stanisz G, Henkelman R. Diffusional anisotropy of T2 components in bovine optic nerve. Magn Reson Med 1998;40:405–410.
7. Reiter DA, Lin PC, Fishbein KW, Spencer RG. Multicomponent T2 relaxation analysis in cartilage. Magn Reson Med 2009;61:803–809.
8. Candes E, Tao T. Near-optimal signal recovery from random projections: Universal encoding strategies? IEEE Trans Inf Theory 2006;52:5406–5425.
9. Donoho D. Compressed sensing. IEEE Trans Inf Theory 2006;52:1289–1306.
10. Gamper U, Boesiger P, Kozerke S. Compressed sensing in dynamic MRI. Magn Reson Med 2008;59:365–373.
11. Jung H, Sung K, Nayak KS, Kim EY, Ye JC. k-t FOCUSS: A general compressed sensing framework for high resolution dynamic MRI. Magn Reson Med 2009;61:103–116.
12. Chen S, Donoho D, Saunders M. Atomic decomposition by basis pursuit. SIAM J Sci Comput 1999;20:33–61.
13. Tropp J, Gilbert A. Signal recovery from random measurements via orthogonal matching pursuit. IEEE Trans Inf Theory 2007;53:4655–4666.

14. Chartrand R. Exact reconstruction of sparse signal via nonconvex minimization. IEEE Signal Process Lett 2007;14:707–710.
15. Aharon M, Elad M, Bruckstein A. K-SVD: An algorithm for designing overcomplete dictionaries for sparse representation. IEEE Trans Signal Process 2006;54:4311–4322.
16. Pati Y, Rezaiifar R, Krishnaprasad P. Orthogonal matching pursuit: Recursive function approximation with applications to wavelet decomposition. In: Proceedings of the 27th annual Asilomar conference on signals, systems and computers; Asilomar Grounds, Pacific Grove, CA, 1993. pp 40–44.
17. Look D, Locker D. Time saving in measurement of NMR and EPR relaxation times. Rev Sci Instrum 1970;41:250–251.
18. Wright J, Ma Y. Dense error correction via ℓ_1 minimization. In: International Conference on acoustics, speech, and signal processing; 2009. pp. 441–444.
19. Doneva M, Sénégas J, Börnert P, Eggers H, Mertins A. Accelerated MR parameter mapping using compressed sensing with model-based sparsifying transform. In: Proceedings of International Society for Magnetic Resonance in Medicine; Honolulu, Hawaii, 2009, Vol. 17, p 2812.
20. Olafsson V, DC N, Fessler J. Fast joint reconstruction of dynamic R2* and field maps in functional MRI. IEEE Trans Med Imaging 2008;27: 1177–1188.